Article

Molecular Dynamics Simulations of Gas Transport Properties in Cross-Linked Polyamide Membranes: Tracing the Morphology and Addition of Silicate Nanotubes

Ehsan Chehrazi*

ACCESS | 📊 Metrics & More | 📰 Article Recommendations

ABSTRACT: This study employs molecular dynamics (MD) simulations to fundamentally provide insight into the role of cross-link density in the CO_2 separation properties of interfacially polymerized polyamide (PA) membranes. For this purpose, two atomistic models of pure polyamide membranes with different cross-link densities are constructed by MD simulations to conceptually determine how the fractional free volume of polyamide affects the gas separation performance of the membrane. The PA membrane with a lower cross-link density (LCPA) shows a higher gas diffusion coefficient, a lower gas solubility coefficient, and a higher gas permeability than the PA membrane with a higher cross-link density (HCPA). Moreover, the pristine and modified silicate nanotubes (SNTs) as the fast gas transport channels are incorporated into the polyamide membranes to assess the effect of the SNT/PA interface chemistry on the CO_2 separation properties of the membranes. SNTs are systematically modified by three modifying agents with different CO_2-philic groups and different interfacial interaction energies with the polyamide matrix. The results of MD simulations demonstrate that the incorporation of silicate nanotubes into the PA matrix increases the gas diffusivity and permeability and decreases the CO_2/gas selectivity. Moreover, the membranes containing modified SNTs possessing high CO_2-philicity and high SNTs/PA interfacial interactions show a high CO_2 separation performance.

1. INTRODUCTION

The global warming by greenhouse gases and the rising demand for natural gas have motivated researchers to find novel materials and new methods to separate carbon dioxide (CO_2) from fuel gas and natural gas, respectively.[1−4] Among various kinds of gas separation methods, polymeric membranes have attracted tremendous attention due to their low cost and easy fabrication process.[5,6] However, the most important point about polymeric membranes is the trade-off between selectivity and permeability that limits the gas separation performance.[7,8]

To overcome the trade-off challenge and improve the gas separation performance, inorganic nanoparticles (NPs) can be incorporated into polymeric membranes, known as mixed matrix membranes (MMMs). There are many types of nanoparticles that can be successfully utilized to prepare MMMs with a considerable enhancement in the CO_2 separation performance.[9−21] Nanoparticles used in MMMs are classified into two distinct groups. Nanoparticles in the first group are intrinsically selective nanoparticles with small-sized pores such as zeolite[9,10] and carbon molecular sieves (CMSs),[11,12] which enhance the CO_2 selectivity of MMMs. Nanoparticles in the second group are porous nanoparticles with large-sized pores that mostly increase the gas permeability of MMMs due to their

rapid gas transport pathways such as carbon nanotubes (CNTs)[13−15] and silicate nanotubes (SNTs).[16−21]

Among different types of nanoparticles, SNTs have demonstrated a significant ability to be utilized in MMMs for gas transport due to their special nanostructural characteristics.[16−21] Embedding SNTs in a less permeable and dense matrix such as cross-linked polyamide, one expects to create rapid gas transport pathways, through the inside of nanotubes, in the membrane. Moreover, SNTs can be modified by different functional groups such as CO_2-philic groups to provide unique features for the adsorption of CO_2 molecules. The modification of the SNT surface with CO_2-philic groups on the one hand facilitates the CO_2 transport through MMMs and on the other hand enhances the SNTs/PA interfacial compatibility. Therefore, the surface modification improves the dispersion of SNTs in the polyamide matrix by enhancing the strength of the interfacial interactions between SNTs and the polyamide.

The experimental methods for evaluating the gas separation performance of MMMs and interfacial interactions between NPs and the polymer matrix are often costly, difficult, and time-consuming.[22,23] To address this problem, molecular dynamics (MD) simulations at a molecular level can offer valuable opportunities to explore a connection between macroscopic properties and microscopic structure.[24−27] The molecular dynamics simulations have been considered as a promising way to provide useful information about the interfacial interactions between NPs and polymer matrix as well as the gas separation properties of mixed matrix membranes.[28−30] However, there is no systematic theoretical investigation in the literature about the effects of different surface modifications of nanoparticles on the NPs/polymer interfacial interactions and gas separation properties of MMMs.

In this work, we study two atomistic models of pure polyamide membranes with different cross-link densities by MD simulations to determine how the fractional free volume of polyamide affects the gas separation properties of membranes. Moreover, systematic theoretical simulations are performed to evaluate the CO_2 separation performance of MMMs containing SNTs with different surface modifications. Furthermore, the SNTs/PA interfacial interactions are quantitatively investigated by MD simulations to assess the effect of the dispersion of different SNTs in the polyamide matrix on the CO_2 separation performance of MMMs.

The nanosized silicate nanotube, SNT, is a type of natural silicate that has the chemical composition of $Al_2(OH)_4Si_2O_5 \cdot nH_2O$. The inner diameter, outer diameter, and length of SNTs are around 20, 70 nm, and 0.1 μm, respectively.[31] Figure 1a,b
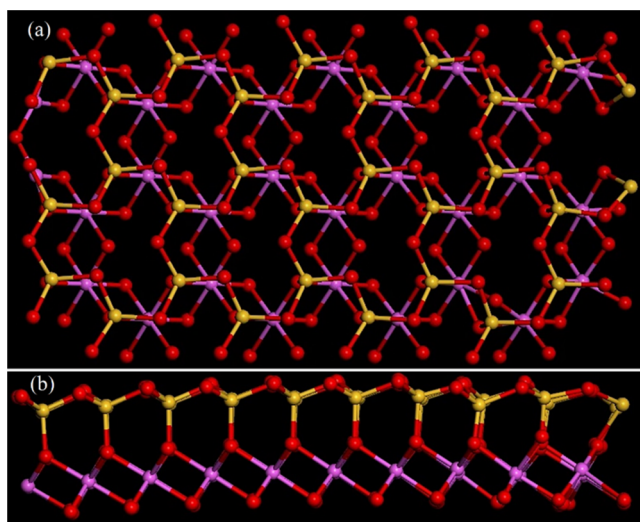
Figure 1. Schematic of silicate nanotubes (SNTs): (a) top view and (b) side view. Red, violet, and yellow atoms are oxygen, aluminum, and silicon, respectively.

exhibits the molecular scheme of the top view and side view of SNTs, respectively. The presence of functional groups on the inner and outer surfaces of SNTs, i.e., aluminol (Al−OH) and siloxane (Si−O−Si),[32−34] respectively, makes SNTs able to modify using the CO_2-philic modifying agents such as silane compounds for CO_2 separation applications.

In this study, three different modifying agents are utilized to simulate the surface modification of SNTs including (i) trimethoxy octyl silane (TOS), (ii) aminoethyl aminopropyl

trimethoxysilane (AEAPTS), and (iii) methacryloxy propyl trimethoxysilane (MPTS) (Table 1). The modified SNTs by the abovementioned modifying agents are named TOS-SNT, AEAPTS-SNT, and MPTS-SNT, respectively.

2. SIMULATION DETAILS

The MD simulations are performed to theoretically investigate different properties of cross-linked polyamide membranes using the Materials Studio software package (version 6.0) published by Accelrys Inc.[35] In addition, the condensed phase optimization molecular potentials for atomistic simulation studies (COMPASS) force field are used to generate the simulations.[36] The total potential energy of a system is simulated using the COMPASS force field, which consists of three parts[3636]

$$E_{total} = E_{valence} + E_{cross\text{-}term} + E_{nonbond} \tag{1}$$

where $E_{valence}$, $E_{cross\text{-}term}$, and $E_{nonbond}$ are valence energy, cross-term energy, and nonbond energy, respectively, which are defined as follows[3636]

$$E_{valence} = E_{bond} + E_{angle} + E_{torsion} + E_{oop} + E_{UB} \tag{2}$$

$$E_{cross\text{-}term} = E_{bond-bond} + E_{angle-angle} + E_{bond-angle} \tag{3}$$
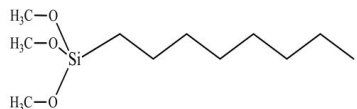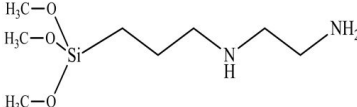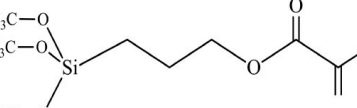
$$E_{nonbond} = E_{vdW} + E_{Coulomb} + E_{H\text{-}bond} \tag{4}$$

The valence energy ($E_{valence}$) has five terms including E_{bond}, E_{angle}, $E_{torsion}$, E_{oop}, and E_{UB}, which are bond stretching, bond angle, bond torsion, out-of-plane interaction, and Urey−Bradley, respectively. The cross-term energy ($E_{cross\text{-}term}$) includes $E_{bond-bond}$, $E_{angle-angle}$, and $E_{bond-angle}$, which are bond−bond stretching, two-angle interaction, and bond−angle interaction, respectively. The nonbond energy ($E_{nonbond}$) is the sum of hydrogen bond energy ($E_{H\text{-}bond}$), van der Waals energy (E_{vdW}), and the Coulomb electrostatic energy ($E_{Coulomb}$).

2.1. Molecular Models. The cross-linked polyamide membranes are constructed by the interfacial polymerization (IP) of an organic monomer, trimesoyl chloride (TMC) and an aqueous monomer, triethylenetetramine (TETA). The simulated chemical structure of constructed cross-linked polyamide using TETA and TMC is shown in Figure 2. It should be noted that the chlorine atoms of the TMC monomers in the polyamide structure may be hydrolyzed to carboxylic acid in the vicinity of the aqueous phase.

2.2. Generation of Cross-Linked Polyamide Membranes. The cross-linked polyamide membranes are generated by interfacial polymerization reaction according to the following procedure: First, TETA and TMC monomers at the atomic level are energetically minimized to obtain reasonable structures. Next, certain amounts of both monomers are packed into a simulation cell using the Amorphous Cell module. The periodic boundary conditions in three dimensions are applied to avoid unwanted boundary terms in the simulation of the membranes. Based on data available in the literature, the density of typical aromatic polyamide prepared by interfacial polymerization is around 1.0 g/cm³.[37,38] Therefore, we set 1.0 g/cm³ as the target density of cross-linked polyamide during the simulations. Then, the simulation cell is energetically minimized and geometrically optimized by Discover and Forcite modules, respectively. After the minimization and optimization, the reactive atoms of aqueous and organic monomers are placed in close proximity to each other. The hydrogen atoms of amine groups of TETA monomers and chlorine atoms of TMC monomers are then

Table 1. Chemical Compositions of the Modifying Agents

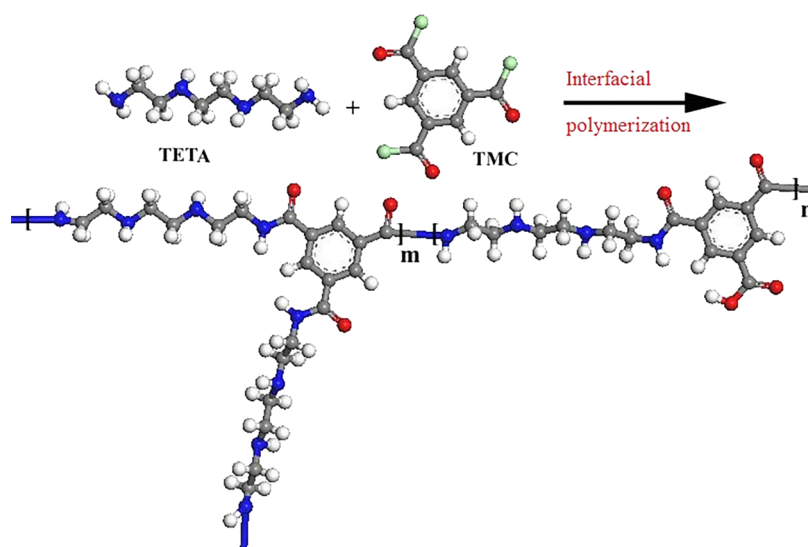| Modifying agents	Molecular structure	Chemical formula
TOS		$CH_3(CH_2)_7Si(OCH_3)_3$
AEAPTS		$(CH_3O)_3Si(CH_2)_3NHCH_2CH_2NH_2$
MPTS		$H_2C=C(CH_3)CO_2(CH_2)_3Si(OCH_3)_3$

Figure 2. Schematic of the interfacial polymerization process of TETA and TMC monomers for the preparation of cross-linked polyamide. White, blue, red, gray, and green atoms are hydrogen, nitrogen, oxygen, carbon, and chlorine, respectively.

removed. According to the IP reaction, the monomers are artificially cross-linked by bridging nitrogen atoms of TETA monomers and carbon atoms of acyl chloride groups of TMC monomers to construct the cross-linked polyamide network. After that, 2000 steps of energy minimization are conducted on the initial cross-linked polyamide network to give the most stable structure. Finally, the molecular dynamics simulations are conducted in the *NVT* ensemble (which is a constant number of particles, volume, and temperature) with the time step of 100 ps to eliminate the hot spots and the undesirable contact such as overlapping. For achieving a more equilibrated system, the cross-linked polyamide network is further conducted by MD simulations in *NPT* ensemble with the time step of 1000 ps. In the *NPT* ensemble, the number of molecules, *N*, pressure, *P*, and the temperature, *T*, of the system are kept constant. To control the pressure (at 1 atm) and temperature (at 298.15 K) of the system, the Andersen barostat and Berendsen thermostat are utilized.[39] The Coulombic interactions are calculated by the Ewald method with the accuracy of 0.001 kcal/mol, and the van der Waals interactions are approximated by the atom-based summation method with a cutoff distance of 12.5 Å (with a spline width of 1 Å and a buffer width of 0.5 Å), where this range

of cutoff distance is less than half of the cell length (around L_x = 26.3 Å, L_y = 26.3 Å, and L_z = 26.3 Å).

The additional MD simulations with the *NVT* ensemble with the time step of 1000 ps are also carried out to relax the final simulated models. According to the explained procedure, two simulated polyamide membranes with different cross-link densities are constructed. The cross-link densities (percentage of part *m* in Figure 2) of low cross-link density polyamide membrane (LCPA) and high cross-link density polyamide membrane (HCPA) are intended to be 20 and 80%, respectively, by varying the ratio of TETA/TMC (22/20 and 28/20, respectively). Therefore, in the first model, the LCPA membrane is composed of 20 TMC monomers and 22 TETA monomers. While 20 TMC monomers and 28 TETA monomers are packed in the simulation cell of the second model (HCPA membrane). Moreover, MMMs are simulated by embedding the pristine and modified SNTs in the LCPA membrane, during the interfacial polymerization of TETA and TMC, based on the procedure described above. The simulation cells including polyamide, different SNTs, and gas molecules are of almost fixed volume with around L_x = 20 Å, L_y = 20 Å, and L_z = 20 Å.

3. RESULTS AND DISCUSSION

3.1. Fractional Free Volume (FFV). The interfacially polymerized LCPA and HCPA membranes have cross-linked structures with different cross-link densities. The mobility of polymer chains is constrained by cross-linking points.[40−42] The cross-link density determines the free volume of polyamide membranes and thus governs the chain mobility and diffusivity of gas molecules through the membranes.

The fractional free volume (FFV) of the polyamide can be theoretically estimated by the MD simulation technique from the Connolly task simulation using different probe diameters[43,44][43,44]

$$FFV = \frac{V_{free}}{V_{free} + V_{occupy}} \tag{5}$$

where V_{occupy} and V_{free} are the occupied volume and the free volume of polyamide, respectively. Figure 3a demonstrates the fractional free volume (FFV) of the simulated LCPA and HCPA membranes. As expected, FFV of LCPA is higher than that of HCPA due to the lower cross-link density of LCPA.

In addition, the pore size distribution (PSD) patterns of two simulated polyamide membranes are obtained by differentiating FFV over the radius of probes (Figure 3b). PSD of the HCPA membrane is narrower than that of the LCPA membrane and is slightly shifted toward lower pore diameters as a result of higher cross-link density. The PSD patterns in Figure 3b reveal that both HCPA and LCPA membranes are dense with the mean pore size around 0.65 and 0.70 Å, respectively, which are lower than the kinetic diameters of CO_2, CH_4, and N_2.

Figure 4 shows the morphology maps of two different cross-linked membranes (LCPA and HCPA). The blue color regions in morphology maps present the free volume of membranes. It is clear from Figure 4a,b that the free volume (blue color regions) in LCPA is higher than that in HCPA, which is in agreement with the results shown in Figure 3a.

Figure 3. (a) Fractional free volume and (b) pore size distributions of LCPA and HCPA.
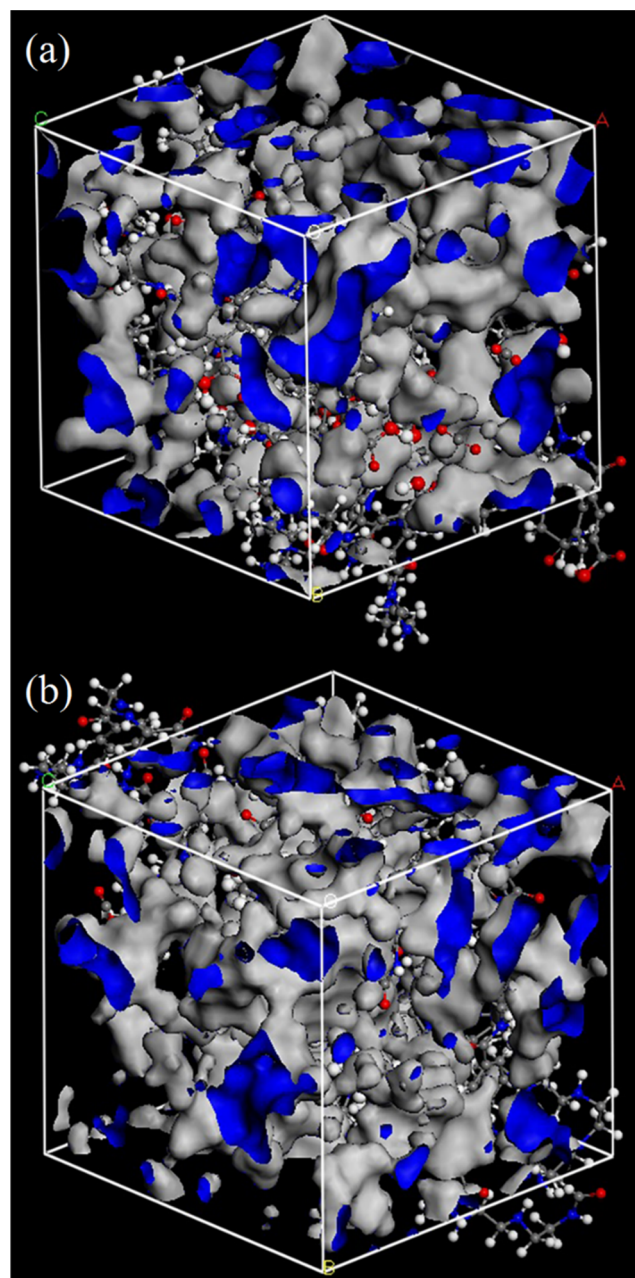
Figure 4. Morphology maps of the free volume in (a) LCPA and (b) HCPA membranes in simulation cells.

3.2. Gas Transport Properties. *3.2.1. Gas Diffusivity.* The diffusion coefficients of CO_2, CH_4, and N_2 molecules through the cross-linked polyamide membranes (HCPA and LCPA) are calculated by analyzing the mean square displacement (MSD) using the molecular dynamics simulations. After equilibration of the simulation cell of the polyamide membrane using different steps of energy minimizing by *NVT* and *NPT* ensemble as described in Section 2.2, three molecules of each gas (N_2, CH_4, and CO_2) are inserted into the simulation cell. Again, 1000,000 steps of *NPT* and *NVT* dynamics are performed to reach the final equilibrium structure. The gas diffusion coefficient is obtained by the slope of MSD of gas molecules plotted against the time of simulation according to the Einstein relation as follows[45,46][45,46]

$$D_A = \frac{1}{6} \lim_{t \to \infty} \frac{d}{dt} \sum_{1}^{n} \langle [R_i(0) - R_i(t)]^2 \rangle \tag{6}$$

where $R_i(0)$ is the position of atom i at time 0 and $R_i(t)$ is the position of atom i at time t, and the average is taken over the whole time period and over all molecules packed in the simulation cell.

Figure 5 presents the MSD curves for N_2, CH_4, and CO_2 diffusion through the simulated interfacially polymerized polyamide membranes during the 1000 ps simulation time. The diffusion coefficients of different gases through the HCPA and LCPA membranes are calculated using the slope of MSD curves (i.e., eq 6) and summarized in Table 2. The gas diffusion coefficients through the cross-linked polyamide membranes vary in the order $N_2 > CH_4 > CO_2$. The diffusion coefficient of gas molecules through a dense membrane is governed by the kinetic diameter of penetrant gas. The kinetic diameter of different gases decreases in the sequence $CH_4 > N_2 > CO_2$.[47−49] It is expected that the smaller penetrant gas shows a higher diffusion coefficient through the dense membrane. Although the CO_2 molecule has a smaller kinetic diameter than CH_4 and N_2, the lowest simulated diffusivity is observed for CO_2. This difference between the trend of kinetic diameters and gas diffusion coefficients obtained by MD simulation can be explained as follows. The CO_2 molecules have a higher affinity toward the polyamide than N_2 and CH_4 molecules because of the strong interactions between CO_2 and CO_2-philic groups of the polyamide such as −COOH, −NH−, and −NHCO− groups. This affinity restricts the diffusion of CO_2 molecules through the simulated polyamide membranes. To confirm this hypothesis, binding energies of penetrant gases to the LCPA membrane are calculated using the COMPASS force field based on eqs 1−4. The results demonstrate that the binding energies are decreased in the order of LCPA-CO_2 (−5276.32 kcal/mol) > LCPA-CH_4 (−4924 kcal/mol) > LCPA-N_2 (−4823.76 kcal/mol), in agreement with the diffusivity results. A similar observation can also be found in the reported works in the literature.[50,51] On the other hand, N_2 has lower interactions with polyamide membranes than CO_2 and CH_4 and shows the highest simulated diffusivity through the polyamide membranes.

Moreover, the diffusivity coefficients of N_2, CH_4, and CO_2 molecules through the LCPA membrane are higher than those through the HCPA membrane due to the higher free volume available for gas diffusion in the LCPA membrane. The MD simulations confirm that the LCPA membrane with lower cross-link density and higher free volume than the HCPA membrane shows higher gas diffusivity.
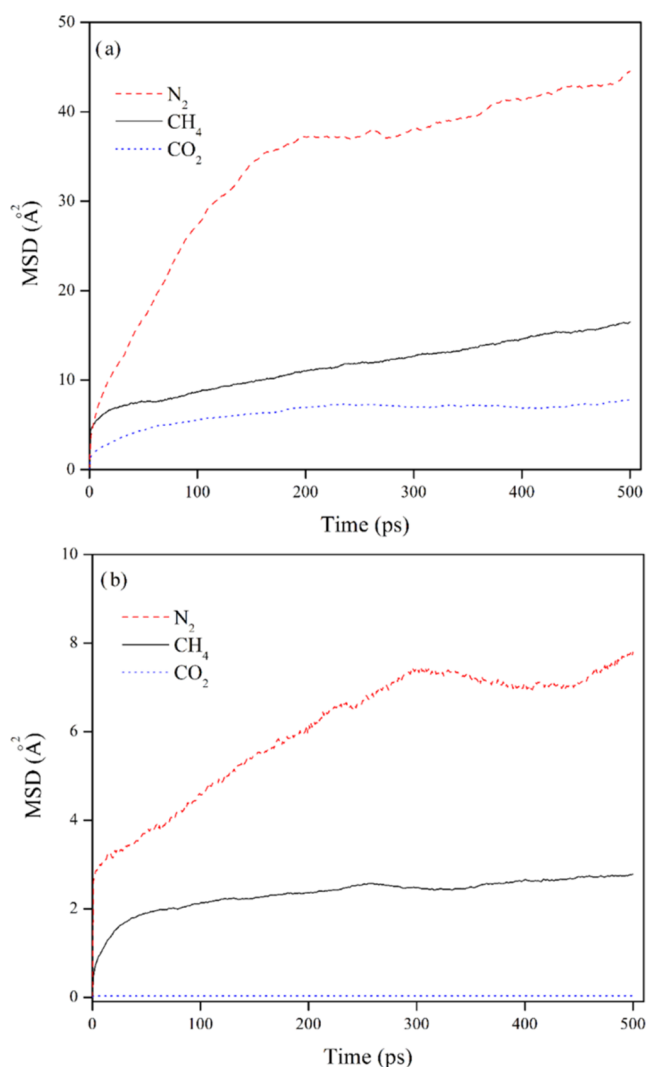

Figure 5. MSD curves of CO_2, N_2, and CH_4 molecules through (a) LCPA and (b) HCPA membranes.

Table 2. Diffusion Coefficients of Different Gases through Polyamide Membranes and MMMs

membranes	diffusivity ($\times 10^{-8}$ cm^2/s)		
	N_2	CH_4	CO_2
HCPA	0.94	0.68	0.59
LCPA	1.38	1.11	1.01
LCPA-SNT	4.30	2.25	2.08
LCPA-TOS-SNT	4.17	2.71	2.25
LCPA-AEAPTS-SNT	4.08	2.23	1.60
LCPA-MPTS-SNT	3.12	2.15	1.53

Table 2 also exhibits that the diffusivity of CO_2, N_2, and CH_4 molecules increases with the addition of the pristine and modified SNTs to the LCPA membrane. SNTs provide rapid transport pathways for gas molecules in MMMs. The CO_2 diffusivity of MMMs increases in the order LCPA-TOS-SNT > LCPA-SNT > LCPA-AEAPTS-SNT > LCPA-MPTS-SNT. It is again evident that the strong interactions between CO_2 and CO_2-philic groups such as AEAPTS and MPTS in modified SNTs restrict CO_2 diffusion.

Therefore, in addition to the transport properties of the polyamide matrix, gas diffusion through SNTs has a crucial role

in determining the final gas diffusion coefficient of MMMs. To evaluate the effect of SNTs on the gas diffusion of MMMs, the gas diffusion mechanisms through SNTs should be accurately ascertained. The gas diffusion through SNTs mainly obeys three mechanisms including Knudsen diffusion, molecular diffusion, and viscous flow.[52] The gas diffusion mechanisms through SNTs are based on the geometry of nanotubes, intrinsic characteristics of gas molecules, and operating conditions such as pressure and temperature. In this case, the inner diameter of SNTs as well as the kinetic diameter of gas molecules mainly determine the dominant gas diffusion mechanism. If the inner diameter of SNTs is smaller than the mean free path (λ) of molecules of gas, the Knudsen diffusion is the dominant mechanism of gas diffusion. The mean free path of molecules of gas is expressed as[52]

$$\lambda = \frac{k_B T}{\sqrt{2}\,\pi\sigma^2 p} \tag{7}$$

where k_B, T, p, and σ are the Boltzmann constant (J/K), the absolute temperature (K), the pressure (Pa), and the kinetic diameter of the gas molecule (m), respectively. In the Knudsen diffusion mechanism, collisions between the gas molecules inside SNTs are less frequent than those between the gas molecules and the inner wall of SNTs. The gas diffusion based on the Knudsen diffusion mechanism is described as[52]

$$D_K = \frac{d}{3}\left(\frac{8RT}{\pi M}\right)^{0.5} \tag{8}$$

where d, R, and M are the inner diameter of SNTs (m), the gas constant (8.314 Pa·m^3/mol·K), and the molecular weight of penetrant gas (kg/mol), respectively. While the inner diameter of SNTs is larger than the mean free path of gas molecules, gas diffusion is governed by molecular diffusion mechanism[52,52]

$$D_M = \frac{3}{8\sigma^2 n}\left(\frac{k_B T}{\pi m}\right)^{0.5} \tag{9}$$

where n is the density of molecule number ($1/m^3$) and m is the gas molecule mass (kg). Moreover, the viscous flow mechanism is important when the SNT diameter is very large or significant pressure is applied between two ends of nanotubes.[52] The gas diffusion through SNTs by viscous flow mechanism is calculated based on the Poiseuille equation[52,52]

$$D_V = \frac{d^2 p}{32\mu} \tag{10}$$

where μ is the viscosity of penetrant gas (Pa·s) and p is the pressure (Pa). The overall gas diffusivity through SNTs is obtained by the combination of three mechanisms based on the dusty gas model[53,53]

$$D_{NT} = \frac{D_K D_M + D_V D_M + D_V D_K}{D_K + D_M} \tag{11}$$

SNTs with an inner diameter of 20 nm render the gas diffusivity (D_{NT}) as high as 1×10^{-2} cm^2/s at a pressure of 2 bar and can significantly increase the overall diffusivity of MMMs. Therefore, the presence of dispersed SNTs in the polyamide matrix has a significant role in increasing the gas diffusion through MMMs.

3.2.2. Gas Solubility. Another important parameter in the gas transport process through polymeric membranes is the solubility of gas molecules in the membranes. The solubility parameter is

proportional to the concentration of adsorbed gas species in the membranes. The concentration of the gas molecules in a polymer is given by the dual-mode sorption (DMS) model. The DMS model describes the equilibrium concentration of adsorbed gas molecules in the polymer, which includes two terms. The first term is related to the dissolution of gas molecules in the dense regions of the polymer (Henry law), and the second term is devoted to the filling of the free volume in the polymer with gas molecules (Langmuir sorption theory). The dual-mode sorption (DMS) model is as follows[54,55,54,55]

$$C_i = C_{Hi} + C_{Li} = k_{Hi}p + \frac{C'_{Li}b_i p}{1 + b_i p} \tag{12}$$

where C_i is the total concentration of gas i adsorbed in the polymer, C_{Hi} presents the Henry sorption, C_{Li} is the Langmuir sorption, k_{Hi} is the Henry law solubility coefficient, C'_{Li} is the Langmuir capacity sorption parameter, b_i is the Langmuir affinity parameter, and p is the pressure.

The concentration of gas molecules adsorbed in the polyamide membrane is obtained using the 10^5 steps of the Grand Canonical Monte Carlo (GCMC) method in the Sorption module, where the chemical potential, volume, and temperature are fixed.[56] Figure 6 demonstrates the simulated adsorption isotherms of different gases in two cross-linked polyamide membranes at the temperature of 298.15 K and in the pressure ranging from 0 to 30 atm. At each pressure, 100,000 steps of GCMC calculations are performed with the initial equilibration period of 10,000 steps.

For both HCPA and LCPA membranes, the concentrations of N_2, CH_4, and CO_2 are linear at low pressures and then deviate from the linear behavior when the pressure increases. The adjustable parameters of eq 12 (k_H, C'_L, and b) are calculated by fitting the DMS model to the concentration−pressure data (Figure 6) using the Levenberg−Marquardt nonlinear regression algorithm and are collected in Table 3.

In both LCPA and HCPA membranes, the capacity of the Langmuir sorption, C'_L, parameter follows the order $N_2 < CH_4 < CO_2$. As can be seen, the C'_L parameter in LCPA is higher than that in HCPA for all penetrant gases. It is mainly attributed to the lower cross-link density and higher free volume available for the adsorption of gas molecules in the LCPA membrane compared with the HCPA membrane. On the other hand, since the Henry law solubility coefficient, k_H, is attributed to the dissolution of gas molecules in the dense regions of the membrane, this parameter is higher for the HCPA membrane than the LCPA membrane for all penetrant gases. It is interesting to note that the k_H parameter of the CO_2 adsorption has the highest value for both LCPA and HCPA membranes in comparison to the N_2 and CH_4 adsorption. These observations are in agreement with the condensability of different gases in a polymer, which is varied in the order $N_2 < CH_4 < CO_2$.[57]

The solubility coefficients (S) of CO_2, CH_4, and N_2 molecules in the polyamide membranes can be calculated by the slope of simulated adsorbed gas concentration against the pressure at zero pressure limit[58,58]

$$S = \lim_{p \to 0} \frac{C_i}{p} \tag{13}$$

where C_i is the gas concentration and p is the pressure. The solubility coefficients of different gases in each membrane (LCPA and HCPA) are obtained using the slope of the curves in Figure 6 at zero pressure and shown in Table 4. The solubility
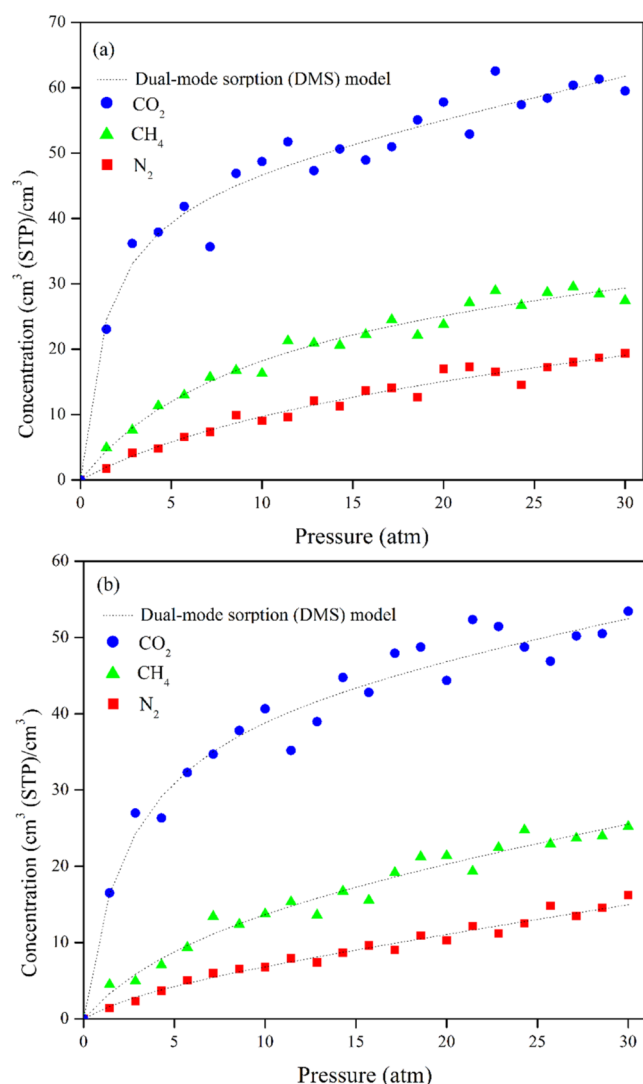
Figure 6. Adsorption isotherms of molecules of CO_2, CH_4, and N_2 in (a) LCPA and (b) HCPA polyamide membranes. The dotted lines represent the model of dual-mode sorption fitted to the data from the GCMC method.

Table 3. Adjustable Parameters of the DMS Model for N_2, CH_4, and CO_2 in LCPA and HCPA Membranes

membranes	gas	k_H (cm^3 (STP)/cm^3 polymer atm)	C'_L (cm^3 (STP)/ cm^3 polymer)	b (atm^{-1})
HCPA	N_2	0.37	4.60	0.22
	CH_4	0.41	16.37	0.14
	CO_2	0.43	48.08	0.31
LCPA	N_2	0.14	20.90	0.07
	CH_4	0.16	31.64	0.11
	CO_2	0.17	64.11	0.29

coefficients of different gases in LCPA and HCPA membranes vary in the order $N_2 < CH_4 < CO_2$, which is in agreement with the increase in the condensability of gas molecules.[57] The solubility of all gases in HCPA is higher than that in LCPA. Therefore, it is further confirmed that the Henry law mechanism is the dominant mechanism of gas solubility in cross-linked polyamide membranes.

The gas solubility coefficients of MMMs containing pristine and modified SNTs are also presented in Table 4. The solubility

Table 4. Solubility Coefficients of Different Gases in Polyamide Membranes and MMMs

	solubility (cm^3 (STP)/cm^3 polymer atm)		
membranes	N_2	CH_4	CO_2
HCPA	1.37	3.16	13.19
LCPA	1.14	2.33	10.68
LCPA-SNT	4.51	10.12	29.92
LCPA-TOS-SNT	4.70	10.44	35.26
LCPA-AEAPTS-SNT	4.86	12.43	52.96
LCPA-MPTS-SNT	4.71	10.61	53.25

coefficients of all gases in MMMs are increased by embedding the pristine and modified SNTs in the order LCPA < LCPA-SNT < LCPA-TOS-SNT < LCPA-AEAPTS-SNT < LCPA-MPTS-SNT. To understand the effect of the incorporation of pristine and modified SNTs into the polyamide matrix on the gas solubility of MMMs, the gas adsorption in pristine and modified SNTs is investigated. The concentration of gas molecules adsorbed in the inner and outer surfaces of pristine and modified SNTs is calculated by 10^5 steps using the Grand Canonical Monte Carlo (GCMC) method in the Sorption module. Figure 7 demonstrates the gas uptake of the pristine and modified SNTs for CO_2, N_2, and CH_4 gases at room temperature and in the pressure range of 0−30 atm. The adsorption isotherms of all gases linearly increase with the pressure at low pressures and then asymptotically approach a limit at high pressures. For modeling the gas adsorption in inorganic particles such as SNTs, the Langmuir model is used[5959]

$$q = \frac{q_m K_L p}{1 + K_L p} \quad \text{original form} \tag{14}$$

where q is the volume of adsorbed gas molecules per specific mass of SNTs (cm^3/g) at pressure p (atm), q_m is the required volume of gas molecules to form a monolayer on the SNT surface (cm^3/g), and K_L is the Langmuir equilibrium or affinity constant (atm^{-1}). By linearizing eq 14 and plotting p/q against p, the parameters q_m and K_L can be obtained

$$\frac{p}{q} = \frac{1}{K_L q_m} + \frac{1}{q_m} p \quad \text{linearized form} \tag{15}$$

Figure 7 also shows the best-fitted curves of the Langmuir model eq 14 to the adsorption isotherms (gas uptake) of N_2, CH_4, and CO_2 for the pristine and modified SNTs. The adjustable parameters in eq 14, i.e., q_m and K_L, for N_2, CH_4, and CO_2, are given in Table 5. As expected, the q_m parameter is higher for CO_2 than CH_4 and N_2 due to the higher condensability of CO_2 molecules.[57] In addition, the larger affinity parameter (K_L) for CO_2 presumably reflects the stronger interactions of CO_2 and SNTs in comparison to the interactions of N_2 and CH_4 with SNTs.

To deeply analyze the effect of surface modification of SNTs on CO_2 adsorption, the CO_2 uptake of different SNTs must be investigated at low pressures. The slope of CO_2 uptake versus pressure at low pressures is a quantitative measure of CO_2 adsorption. Figure 8 shows the CO_2 uptake of pristine and modified SNTs at low pressures (<1.2 atm). The adsorption of CO_2 by different SNTs increases in the order pristine SNT < TOS-SNT < AEAPTS-SNT < MPTS-SNT. It means that the surface modification increases the affinity of SNTs toward CO_2 molecules. The amine groups in the AEAPTS modifier and oxygen-containing groups in the MPTS modifier are the
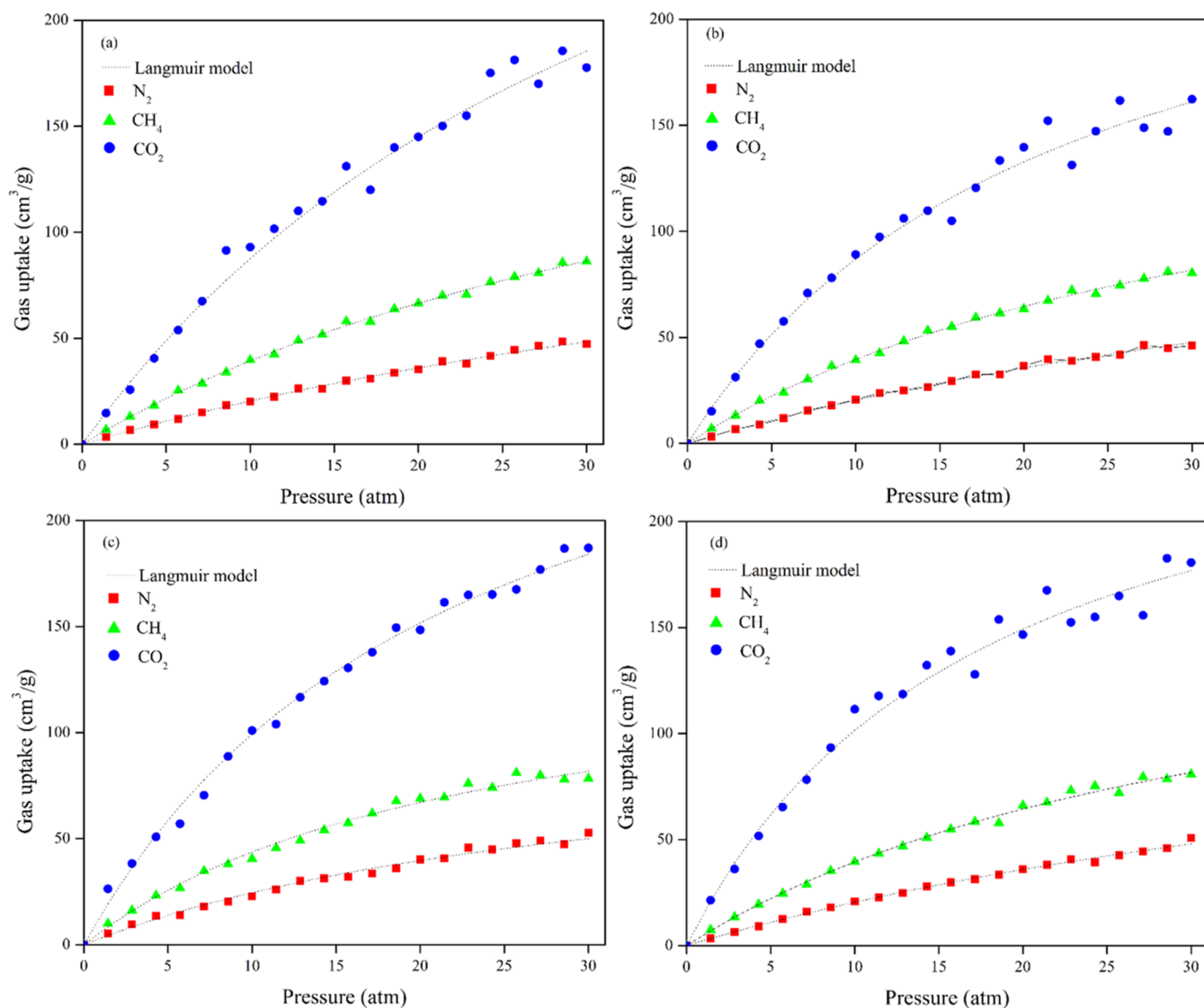
Figure 7. Adsorption isotherm data of different gases in (a) pristine SNT, (b) TOS-SNT, (c) AEAPTS-SNT, and (d) MPTS-SNT using the GCMC method. The dotted lines represent the Langmuir model fitted to the data.

Table 5. Fitting Parameters of the Langmuir Model for the Adsorption of Different Gases in Pristine and Modified SNTs

nanotubes	gas	K_L (atm^{-1})	q_m (cm^3/g)
pristine SNT	N_2	1.50×10^{-2}	153.3
	CH_4	2.20×10^{-2}	214.9
	CO_2	2.60×10^{-2}	419.3
TOS-SNT	N_2	1.60×10^{-2}	145.2
	CH_4	2.90×10^{-2}	174.5
	CO_2	4.50×10^{-2}	280.3
AEAPTS-SNT	N_2	3.10×10^{-2}	104.4
	CH_4	4.30×10^{-2}	144.7
	CO_2	4.50×10^{-2}	321.4
MPTS-SNT	N_2	1.60×10^{-2}	146.6
	CH_4	2.90×10^{-2}	175.3
	CO_2	5.60×10^{-2}	281.6

preferential adsorption sites for the CO_2 molecules. The increasing trend of solubility coefficients in MMMs (Table 4) is in a positive direction, with the increasing trend of CO_2 uptake by the pristine or modified SNTs.
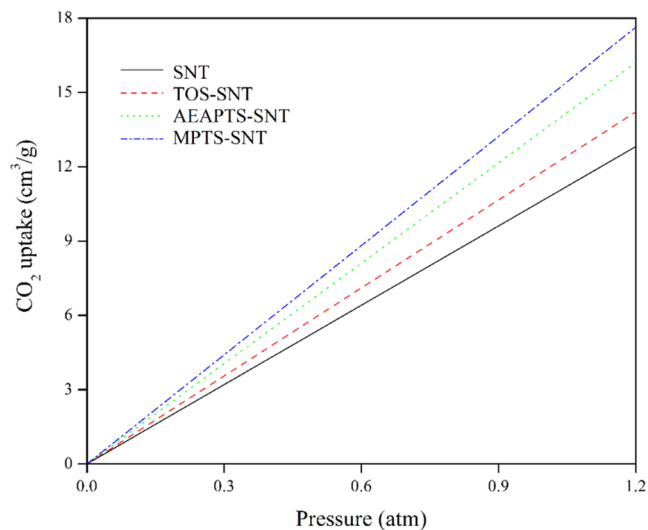
Figure 8. CO_2 adsorption isotherms of pristine and modified SNTs at low pressures.

To gain deeper insight into the interactions between CO_2 and interfacially polymerized polyamide, the radial distribution function is calculated using molecular dynamics simulations. The probability of finding a pair of atoms in a distance r from each other relative to the probability for a random distribution is presented by the radial distribution function (RDF), $g(r)$ as[30,60]

$$g_{ij}(r) = \frac{1}{\rho_{ij} N_{ij} 4\pi r^2 L}\left(\sum_{a=1}^{L}\sum_{b=1}^{N_{ij}} \Delta N_{ij}(r \rightarrow r_i + \delta r)\right) \quad (16)$$

where N_{ij} is the number of all atoms (i and j) in the simulation cell. In addition, L, δr, ΔN_{ij}, and ρ_{ij} are the number of time steps, the distance interval, the number of j (or i) atoms between r and $r + \delta r$ around an i (or j) atom, and the density of polymer bulk, respectively.

The radial distribution functions (RDF) between the CO_2 molecules and different atoms of the polyamide, $g(r)$, are shown in Figure 9. The position of each peak in $g(r)$ gives the
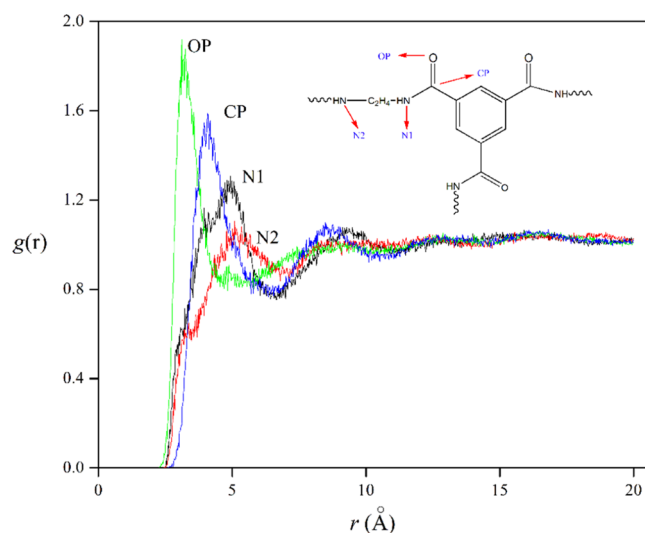
Figure 9. Radial distribution functions $g(r)$ between CO_2 and different atoms of the polyamide membrane.

interaction interval between the nearest pairs of atoms in the system. Figure 9 exhibits the $g(r)$ related to the CO_2 interactions with four different atoms in the structure of the cross-linked polyamide including the nitrogen, carbon, and oxygen atoms of the amide group (named N1, CP, and OP, respectively) and nitrogen atoms in the backbone of polyamide (N2) (see the inset of Figure 9). The highest peak appears at 3.11 Å, which corresponds to the interactions of CO_2 molecules with oxygen atoms of amide groups (OP). This observation indicates that the

oxygen atoms in the polyamide structure have the most attractive interactions with the CO_2 molecules.

In addition, the CO_2–CP, CO_2–N1, and CO_2–N2 peaks have been located at 4.07, 4.93, and 5.09 Å, respectively. Therefore, the energies of interactions between the CO_2 molecules and different atoms in the polyamide structure increase in the order N2 < N1 < CP < OP. Therefore, the atoms of amide groups in the polyamide membrane are the preferential sites for the adsorption of CO_2 molecules.

3.2.3. Gas Permeability. The gas permeability through the dense polyamide membranes is described by the solution–diffusion model.[61] The gas permeability through the membrane is calculated by the product of the diffusion coefficient and solubility coefficient as follows[62,62]

$$P = D \times S \quad (17)$$

where the gas permeability of the membrane (P) is expressed in the Barrer unit (1 Barrer = 7.6×10^{-9} cm^3 (STP) cm/cm^2 polymer atm). Also, S (cm^3 (STP)/cm^3 polymer atm) and D (cm^2/s) are the solubility coefficient and diffusivity coefficient, respectively. In addition, selectivity is defined as the relative permeability of the gas species.

The simulated gas permeabilities through the polyamide membranes for CO_2, CH_4, and N_2 are shown in Table 6. The gas permeability values of all gases in the LCPA membrane are higher than those in the HCPA membrane. The reason for this behavior is the lower cross-link density and higher free volume of LCPA in comparison to HCPA. The gas permeabilities through the polyamide membranes for different gases are increased in the order CO_2 > CH_4 > N_2. Although the diffusivity of CO_2 is the lowest among other gases, the higher value of the CO_2 solubility is responsible for the higher value of the CO_2 permeability.

Moreover, the gas permeability values of LCPA-based MMMs are investigated to elucidate the effects of pristine and modified SNTs on the gas permeation of MMMs. The permeability values of N_2, CH_4, and CO_2 through LCPA MMMs containing the pristine and modified SNTs are calculated using eq 17 and shown in Table 6. The gas permeability values of all MMMs are higher than that of the pure LCPA membrane due to the presence of rapid transport pathways through pristine and modified SNTs. The CO_2 permeability of MMMs is increased in the order LCPA-SNT < LCPA-TOS-SNT < LCPA-MPTS-SNT < LCPA-AEAPTS-SNT. The grafting of MPTS and AEAPTS modifying agents on the surface of SNTs increases the CO_2 permeability of MMMs more than grafting of the TOS modifying agent on the surface of SNTs due to the high CO_2-philicity of MPTS and AEAPTS modifying agents. Although the CO_2 adsorption of MPTS-SNT is higher than that of AEAPTS-SNT (Figure 8), the higher CO_2 permeability of LCPA-AEAPTS-SNT than that of LCPA-MPTS-SNT is due to the better dispersion of AEAPTS-SNTs in the polyamide matrix,

Table 6. Permeability of Different Gases through Polyamide Membranes and MMMs

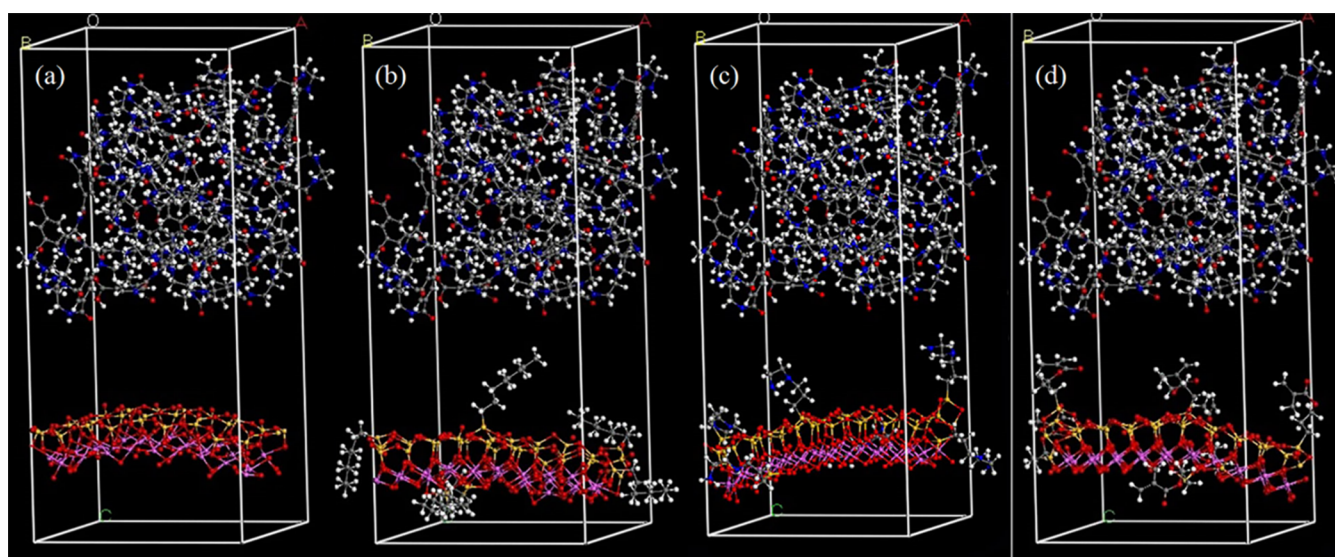| membranes	permeability (Barrer)			selectivity	
	N_2	CH_4	CO_2	CO_2/N_2	CO_2/CH_4
HCPA	1.69	2.81	10.18	6.02	3.62
LCPA	2.08	3.39	14.24	6.85	4.20
LCPA-SNT	25.60	30.00	81.90	3.20	2.73
LCPA-TOS-SNT	25.79	37.30	104.00	4.03	2.79
LCPA-AEAPTS-SNT	26.10	36.40	112.00	4.29	3.08
LCPA-MPTS-SNT	19.40	30.10	107.00	5.52	3.55

Figure 10. Simulation models of MMMs containing (a) pristine SNTs, (b) TOS-SNTs, (c) AEAPTS-SNTs, and (d) MPTS-SNTs.

Table 7. Interaction Energies between the Polyamide and SNTs in MMMs

interaction energy (kcal/mol)	SNT/PA	TOS-SNT/PA	MPTS-SNT/PA	AEAPTS-SNT/PA
total energy	−83.86	−3121.66	−12,413.11	−21,787.83
valence energy	−1.64	256.35	1264.47	2283.55
cross terms	−27.34	−15.13	−9.18	−15.32
nonbond energy	−54.78	−3362.79	−13,668.41	−24,056.06

which is described in the next section. Therefore, the gas permeation of mixed matrix membranes is dependent not only on the properties of the polyamide matrix and SNT characteristics but also on the CO_2-philicity of modifying agents and interfacial interactions at the SNTs/PA interface.

In addition, the CO_2/N_2 and CO_2/CH_4 selectivities of MMMs containing the pristine and modified SNTs increase in the order LCPA-SNT < LCPA-TOS-SNT < LCPA-AEAPTS-SNT < LCPA-MPTS-SNT. The highest CO_2/gas selectivity of LCPA-MPTS-SNT is related to the higher CO_2 adsorption at the MPTS-SNT/PA interface.

3.3. SNTs/PA Interfacial Interactions. To analyze the interfacial interactions between the polyamide matrix, molecular dynamics simulations are also employed between the polyamide matrix prepared by interfacial polymerization and the pristine or modified SNTs. The interaction energy, ΔE, between the polyamide (PA) and SNTs is calculated as follows[63]

$$\Delta E = E_{SNT/PA} - (E_{PA} + E_{SNT}) \quad (18)$$

where $E_{SNT/PA}$ is the total potential energy of SNTs/PA MMM. In addition, E_{SNT} and E_{PA} are the potential energies of SNTs and polyamide, respectively. Figure 10 schematically exhibits four simulation models of MMMs containing pristine and modified SNTs with different surface modifications. It is important to note that a slice of SNTs in the vicinity of the polyamide is shown in Figure 10.

The SNTs/PA interfacial interaction energies of simulation models are obtained by COMPASS force field based on eqs 1−4 and the results are summarized in Table 7. The interfacial interaction energy values of modified SNTs/PA are significantly higher than that of pristine SNT/PA and increase in the order pristine SNT/PA < TOS-SNT/PA < MPTS-SNT/PA < AEAPTS-SNT/PA. The modifying agents at the SNTs/PA

interface increase the compatibility of SNTs with the PA matrix. The high interfacial interaction energy in MPTS-SNT/PA is mainly due to the formed hydrogen bonds between oxygen-containing groups of MPTS and the amine groups of polyamide. In addition, the substantially high value of AEAPTS-SNT/PA interfacial interaction energy might be due to the formation of covalent bonds between amine groups of AEAPTS and acyl chloride groups of TMC monomers in the organic phase prior to the interfacial polymerization process.[64,65] The higher interfacial interaction energy leads to the stronger adhesion between the polyamide and modified SNTs and, therefore, the better dispersion of modified SNTs within the polyamide matrix.

4. CONCLUSIONS

In this study, two interfacially polymerized membranes with different cross-link densities were generated using molecular dynamics simulations. The membrane with the lower cross-link density (LCPA) possessed a higher fractional free volume (FFV) than the membrane with the higher cross-link density (HCPA). Therefore, the LCPA membrane with higher FFV showed a higher gas diffusion coefficient, lower gas solubility coefficient, and higher gas permeability than the HCPA membrane. Moreover, MMMs were simulated by embedding pristine and modified silicate nanotubes (SNTs) in the LCPA membrane. The results of MD simulations exhibit that the presence of silicate nanotubes in the PA matrix increases the gas diffusivity coefficient. The presence of pristine and modified SNTs increased the CO_2 permeability through MMMs in the order LCPA-SNT < LCPA-TOS-SNT < LCPA-MPTS-SNT < LCPA-AEAPTS-SNT. However, the presence of large-diameter SNTs decreases the CO_2/gas selectivity values due to an increase of FFV in the membranes. Furthermore, MMM containing MPTS-SNTs shows the highest CO_2/gas selectivity

due to the high CO_2 adsorption at the MPTS-SNT/PA interface. This fact shows that the grafting of different side groups able to specific interactions with CO_2 to the surface of SNT does not result in a sufficient increase of CO_2 solubility to overcome the effect of diffusion selectivity decrease.

The results of MD simulations demonstrated that the oxygen atoms of amide groups in the structure of polyamide chains have the most attractive interactions with the CO_2 molecules. The MD simulations also showed that the grafting of modifying agents on the SNT surface improves the SNTs/PA interfacial compatibility. In addition, the SNTs/PA interfacial interaction energy values in different MMMs increased in the order pristine SNT/PA < TOS-SNT/PA < MPTS-SNT/PA < AEAPTS-SNT/PA.

■ AUTHOR INFORMATION

Corresponding Author

Ehsan Chehrazi − *Department of Polymer Chemistry and Materials, Faculty of Chemistry and Petroleum Sciences, Shahid Beheshti University, Tehran 1983969411, Iran;* orcid.org/0000-0001-7008-1799; Email: e_chehrazi@sbu.ac.ir

Complete contact information is available at:
https://pubs.acs.org/10.1021/acsomega.3c10108

Notes
The author declares no competing financial interest.

■ ACKNOWLEDGMENTS

■ REFERENCES

(1) Ramírez-Santos, Á. A.; Castel, C.; Favre, E. Utilization of blast furnace flue gas: Opportunities and challenges for polymeric membrane gas separation processes. *J. Membr. Sci.* 2017, 526, 191−204.
(2) Lakhi, K. S.; Park, D.-H.; Singh, G.; Talapaneni, S. N.; Ravon, U.; Al-Bahily, K.; Vinu, A. Energy efficient synthesis of highly ordered mesoporous carbon nitrides with uniform rods and their superior CO2 adsorption capacity. *J. Mater. Chem. A* 2017, 5 (31), 16220−16230.
(3) Elmobarak, W. F.; Almomani, F.; Tawalbeh, M.; Al-Othman, A.; Martis, R.; Rasool, K. Current status of CO2 capture with ionic liquids: Development and progress. *Fuel* 2023, 344, No. 128102.
(4) Halawy, S. A.; Osman, A. I.; Nasr, M.; Rooney, D. W. Mg−O−F Nanocomposite Catalysts Defend against Global Warming via the Efficient, Dynamic, and Rapid Capture of CO2 at Different Temperatures under Ambient Pressure. *ACS Omega* 2022, 7 (43), 38856−38868.
(5) Sandru, M.; Sandru, E. M.; Ingram, W. F.; Deng, J.; Stenstad, P. M.; Deng, L.; Spontak, R. J. An integrated materials approach to ultrapermeable and ultraselective CO2 polymer membranes. *Science* 2022, 376 (6588), 90−94.
(6) Sekizkardes, A. K.; Kusuma, V. A.; McNally, J. S.; Gidley, D. W.; Resnik, K.; Venna, S. R.; Hopkinson, D. Microporous polymeric composite membranes with advanced film properties: pore intercalation yields excellent CO2 separation performance. *J. Mater. Chem. A* 2018, 6 (45), 22472−22477.
(7) Robeson, L. M.; Liu, Q.; Freeman, B. D.; Paul, D. R. Comparison of transport properties of rubbery and glassy polymers and the relevance to the upper bound relationship. *J. Membr. Sci.* 2015, 476, 421−431.
(8) Robeson, L. M. The upper bound revisited. *J. Membr. Sci.* 2008, 320 (1−2), 390−400.
(9) Zagho, M. M.; Hassan, M. K.; Khraisheh, M.; Al-Maadeed, M. A. A.; Nazarenko, S. A review on recent advances in CO2 separation using zeolite and zeolite-like materials as adsorbents and fillers in mixed matrix membranes (MMMs). *Chem. Eng. J. Adv.* 2021, 6, No. 100091.
(10) Chuah, C. Y.; Lee, J.; Bao, Y.; Song, J.; Bae, T.-H. High-Performance Porous Carbon-Zeolite Mixed-Matrix Membranes for CO2/N2 Separation. *J. Membr. Sci.* 2021, 622, No. 119031.
(11) Wiryoatmojo, A. S.; Mannan, H. A.; Nasir, R.; Mukhtar, H.; Mohshim, D. F.; Abdulrahman, A.; Man, Z. Surface modification effect of carbon molecular sieve (CMS) on the morphology and separation performance of mixed matrix membranes. *Polym. Test.* 2019, 80, No. 106152.
(12) Guo, A.; Ban, Y.; Yang, K.; Zhou, Y.; Cao, N.; Zhao, M.; Yang, W. Molecular sieving mixed matrix membranes embodying nano-fillers with extremely narrow pore-openings. *J. Membr. Sci.* 2020, 601, No. 117880.
(13) Borgohain, R.; Jain, N.; Prasad, B.; Mandal, B.; Su, B. Carboxymethyl chitosan/carbon nanotubes mixed matrix membranes for CO2 separation. *React. Funct. Polym.* 2019, 143, No. 104331.
(14) Amirkhani, F.; Mosadegh, M.; Asghari, M.; Parnian, M. J. The beneficial impacts of functional groups of CNT on structure and gas separation properties of PEBA mixed matrix membranes. *Polym. Test.* 2020, 82, No. 106285.
(15) Zhang, H.; Guo, R.; Hou, J.; Wei, Z.; Li, X. Mixed-matrix membranes containing carbon nanotubes composite with hydrogel for efficient CO2 separation. *ACS Appl. Mater. Interfaces* 2016, 8 (42), 29044−29051.
(16) Ismail, A. F.; Hashemifard, S.; Matsuura, T. Facilitated transport effect of Ag+ ion exchanged halloysite nanotubes on the performance of polyetherimide mixed matrix membrane for gas separation. *J. Membr. Sci.* 2011, 379 (1), 378−385.
(17) Wong, K.; Goh, P.; Ismail, A. Gas Separation Performance of Thin Film Nanocomposite Membranes Incorporated with Polymethyl Methacrylate Grafted Multi-Walled Carbon Nanotubes. *Int. Biodeterior. Biodegrad.* 2015, 102, 339−345.
(18) Wong, K. C.; Goh, P.; Ng, B.; Ismail, A. Thin film nanocomposite embedded with polymethyl methacrylate modified multi-walled carbon nanotubes for CO2 removal. *RSC Adv.* 2015, 5 (40), 31683−31690.
(19) Hashemifard, S.; Ismail, A.; Matsuura, T. Mixed matrix membrane incorporated with large pore size halloysite nanotubes (HNTs) as filler for gas separation: morphological diagram. *Chem. Eng. J.* 2011, 172 (1), 581−590.
(20) Murali, R. S.; Padaki, M.; Matsuura, T.; Abdullah, M.; Ismail, A. Polyaniline in situ modified halloysite nanotubes incorporated asymmetric mixed matrix membrane for gas separation. *Sep. Purif. Technol.* 2014, 132, 187−194.
(21) Rafiq, S.; Saeed, M.; Jamil, A.; Rashid, M. I.; Irfan, M.; Iqbal, T.; Inayat, A.; Jamil, F.; Iqbal, J.; Khurram, M. S.; Mehadi, M. S. Advances in Halloysite Nanotubes (HNTs)-Based Mixed-Matrix Membranes for CO2 Capture. *ChemBioEng Rev.* 2023, 10, 480−490, DOI: 10.1002/cben.202200041.
(22) Salahshoori, I.; Seyfaee, A.; Babapoor, A. Recent advances in synthesis and applications of mixed matrix membranes. *Synth. Sintering* 2021, 1 (1), 1−27.
(23) Hu, L.; Clark, K.; Alebrahim, T.; Lin, H. Mixed matrix membranes for post-combustion carbon capture: From materials design to membrane engineering. *J. Membr. Sci.* 2022, 644, No. 120140.
(24) Bisoi, S.; Mandal, A. K.; Padmanabhan, V.; Banerjee, S. Aromatic polyamides containing trityl substituted triphenylamine: Gas transport properties and molecular dynamics simulations. *J. Membr. Sci.* 2017, 522, 77−90.
(25) Balçık, M.; Tantekin-Ersolmaz, S. B.; Ahunbay, M. G. Interfacial analysis of mixed-matrix membranes under exposure to high-pressure CO2. *J. Membr. Sci.* 2020, 607, No. 118147.
(26) Liu, Y.-C.; Chen, C.-Y.; Lin, G.-S.; Chen, C.-H.; Wu, K. C.-W.; Lin, C.-H.; Tung, K.-L. Characterization and molecular simulation of Pebax-1657-based mixed matrix membranes incorporating MoS2 nanosheets for carbon dioxide capture enhancement. *J. Membr. Sci.* 2019, 582, 358−366.
(27) Asif, K.; Lock, S. S. M.; Taqvi, S. A. A.; Jusoh, N.; Yiin, C. L.; Chin, B. L. F. A molecular simulation study on amine-functionalized

silica/polysulfone mixed matrix membrane for mixed gas separation. *Chemosphere* **2023**, *311*, No. 136936.

(28) Ming, Y.; Zhou, Z.; Hao, T.; Nie, Y. Polymer Nanocomposites: Role of modified filler content and interfacial interaction on crystallization. *Eur. Polym. J.* **2022**, *162*, No. 110894.

(29) Deng, J.; Song, Y.; Lan, Z.; Xu, Z.; Chen, Y.; Yang, B.; Hao, H. The surface modification effect on the interfacial properties of glass fiber-reinforced epoxy: A molecular dynamics study. *Nanotechnol. Rev.* **2022**, *11* (1), 1143−1157.

(30) Chehrazi, E.; Taheri-Qazvini, N. Segmental dynamics and cooperativity length of PMMA/SAN miscible blend intercalated in organically modified nanoclay. *Langmuir* **2018**, *34* (47), 14358−14367.

(31) Hashemifard, S.; Ismail, A.; Matsuura, T. Mixed matrix membrane incorporated with large pore size halloysite nanotubes (HNT) as filler for gas separation: experimental. *J. Colloid Interface Sci.* **2011**, *359* (2), 359−370.

(32) Carli, L. N.; Daitx, T. S.; Soares, G. V.; Crespo, J. S.; Mauler, R. S. The effects of silane coupling agents on the properties of PHBV/halloysite nanocomposites. *Appl. Clay Sci.* **2014**, *87*, 311−319.

(33) Wan, X.; Zhan, Y.; Zeng, G.; He, Y. Nitrile functionalized halloysite nanotubes/poly (arylene ether nitrile) nanocomposites: interface control, characterization, and improved properties. *Appl. Surf. Sci.* **2017**, *393*, 1−10.

(34) Radha, A.; Wang, S.-F. Designing Hybrid Lanthanum Stannate/Functionalized Halloysite Nanotubes as Electrode Material for Electrochemical Detection of 4-(Methylamino) phenol (Metol) in Environmental Samples. *ACS Sustainable Chem. Eng.* **2023**, *11* (13), 5072−5081.

(35) *Materials Studio Release Notes*, Release 6.0; Accelrys Software Inc.: San Diego, 2011.

(36) Sun, H. COMPASS: an ab initio force-field optimized for condensed-phase applications overview with details on alkane and benzene compounds. *J. Phys. Chem. B* **1998**, *102* (38), 7338−7364.

(37) Kotelyanskii, M.; Wagner, N.; Paulaitis, M. Atomistic simulation of water and salt transport in the reverse osmosis membrane FT-30. *J. Membr. Sci.* **1998**, *139* (1), 1−16.

(38) Zhang, X.; Cahill, D. G.; Coronell, O.; Mariñas, B. J. Absorption of water in the active layer of reverse osmosis membranes. *J. Membr. Sci.* **2009**, *331* (1−2), 143−151.

(39) Wang, X.-Y.; Hill, A. J.; Freeman, B. D.; Sanchez, I. C. Structural, sorption and transport characteristics of an ultrapermeable polymer. *J. Membr. Sci.* **2008**, *314* (1−2), 15−23.

(40) Chehrazi, E.; Qazvini, N. T. Nanoconfined segmental dynamics in miscible polymer blend nanocomposites: the influence of the geometry of nanoparticles. *Iran. Polym. J.* **2013**, *22* (8), 613−622.

(41) Qazvini, N. T.; Chehrazi, E. Glass transition behavior and dynamic fragility of PMMA-SAN miscible blend-clay nanocomposites. *J. Macromol. Sci., Part B* **2011**, *50* (11), 2165−2177.

(42) Shen, J.; Lin, X.; Liu, J.; Li, X. Effects of cross-link density and distribution on static and dynamic properties of chemically cross-linked polymers. *Macromolecules* **2019**, *52* (1), 121−134.

(43) Velioğlu, S.; Tantekin-Ersolmaz, S. B.; Chew, J. W. Towards the generalization of membrane structure-property relationship of polyimides and copolyimides: A group contribution study. *J. Membr. Sci.* **2017**, *543*, 233−254.

(44) Mazlan, N.; Jusoh, N.; Lock, S. S. M. Investigation of transport properties of 6FDA-durene polymeric membrane for landfill gas application using molecular simulation approach. *Chemosphere* **2022**, *307*, No. 136019.

(45) Ledesma-Durán, A.; Juárez-Valencia, L. H. Diffusion coefficients and MSD measurements on curved membranes and porous media. *Eur. Phys. J. E* **2023**, *46* (8), No. 70.

(46) Hung, T.-H.; Deng, X.; Lyu, Q.; Lin, L.-C.; Kang, D.-Y. Coulombic effect on permeation of CO2 in metal-organic framework membranes. *J. Membr. Sci.* **2021**, *639*, No. 119742.

(47) Karakiliç, P.; Huiskes, C.; Luiten-Olieman, M. W.; Nijmeijer, A.; Winnubst, L. Sol-gel processed magnesium-doped silica membranes with improved H2/CO2 separation. *J. Membr. Sci.* **2017**, *543*, 195−201.

(48) Chehrazi, E. Theoretical models for gas separation prediction of mixed matrix membranes: effects of the shape factor of nanofillers and interface voids. *J. Polym. Eng.* **2023**, *43* (3), 287−296.

(49) Chehrazi, E. gas permeation model for mixed matrix membranes: the new renovated Maxwell model. *Compos. Interfaces* **2023**, *30*, 899−908.

(50) Chang, K.-S.; Wu, Z.-C.; Kim, S.; Tung, K.-L.; Lee, Y. M.; Lin, Y.-F.; Lai, J.-Y. Molecular modeling of poly (benzoxazole-co-imide) membranes: A structure characterization and performance investigation. *J. Membr. Sci.* **2014**, *454*, 1−11.

(51) Golzar, K.; Amjad-Iranagh, S.; Amani, M.; Modarress, H. Molecular simulation study of penetrant gas transport properties into the pure and nanosized silica particles filled polysulfone membranes. *J. Membr. Sci.* **2014**, *451*, 117−134.

(52) Chehrazi, E.; Raef, M.; Noroozi, M.; Panahi-Sarmad, M. A Theoretical Model for the Gas Permeation Prediction of Nanotube-Mixed Matrix Membranes; Unveiling the Effect of Interfacial Layer. *J. Membr. Sci.* **2019**, *570−571*, 168−175.

(53) Lee, J.-G.; Lee, E.-J.; Jeong, S.; Guo, J.; An, A. K.; Guo, H.; Kim, J.; Leikness, T.; Ghaffour, N. Theoretical modeling and experimental validation of transport and separation properties of carbon nanotube electrospun membrane distillation. *J. Membr. Sci.* **2017**, *526*, 395−408.

(54) Lin, R.; Ge, L.; Liu, S.; Rudolph, V.; Zhu, Z. Mixed-matrix membranes with metal−organic framework-decorated CNT fillers for efficient CO2 separation. *ACS Appl. Mater. Interfaces* **2015**, *7* (27), 14750−14757.

(55) Saberi, M.; Rouhi, P.; Teimoori, M. Estimation of dual mode sorption parameters for CO2 in the glassy polymers using group contribution approach. *J. Membr. Sci.* **2020**, *595*, No. 117481.

(56) Velioglu, S.; Keskin, S. Simulation of H 2/CH 4 mixture permeation through MOF membranes using non-equilibrium molecular dynamics. *J. Mater. Chem. A* **2019**, *7* (5), 2301−2314.

(57) Zhao, H.; Ding, X.; Yang, P.; Li, L.; Li, X.; Zhang, Y. A novel multi-armed and star-like poly (ethylene oxide) membrane for CO2 separation. *J. Membr. Sci.* **2015**, *489*, 258−263.

(58) Ramdin, M.; Balaji, S. P.; Vicent-Luna, J. M.; Gutiérrez-Sevillano, J. J.; Calero, S.; de Loos, T. W.; Vlugt, T. J. Solubility of the precombustion gases CO2, CH4, CO, H2, N2, and H2S in the ionic liquid [bmim][Tf2N] from Monte Carlo simulations. *J. Phys. Chem. C* **2014**, *118* (41), 23599−23604.

(59) Qiu, N.; Bai, X.; Xu, J.; Sun, N.; Francisco, J. S.; Yang, M.; Huang, Q.; Du, S. Adsorption behaviors and phase equilibria for clathrate hydrates of sulfur-and nitrogen-containing small molecules. *J. Phys. Chem. C* **2019**, *123* (5), 2691−2702.

(60) Sunda, A. P.; Singh, S.; Yadav, S.; Singh, R. K. Atomistic Simulations of Hydrated Sulfonated Polybenzophenone Block Copolymer Membranes. *ChemPhysChem* **2023**, *24* (16), No. e202300104.

(61) Gao, Y.; Qiao, Z.; Zhao, S.; Wang, Z.; Wang, J. In situ synthesis of polymer grafted ZIFs and application in mixed matrix membrane for CO 2 separation. *J. Mater. Chem. A* **2018**, *6* (7), 3151−3161.

(62) Weidman, J. R.; Luo, S.; Doherty, C. M.; Hill, A. J.; Gao, P.; Guo, R. Analysis of governing factors controlling gas transport through fresh and aged triptycene-based polyimide films. *J. Membr. Sci.* **2017**, *522*, 12−22.

(63) Steinmann, C.; Olsson, M. A.; Ryde, U. Relative ligand-binding free energies calculated from multiple short QM/MM MD simulations. *J. Chem. Theory Comput.* **2018**, *14* (6), 3228−3237.

(64) Yu, S.; Li, S.; Huang, S.; Zeng, Z.; Cui, S.; Liu, Y. Covalently bonded zeolitic imidazolate frameworks and polymers with enhanced compatibility in thin film nanocomposite membranes for gas separation. *J. Membr. Sci.* **2017**, *540*, 155−164.

(65) Asempour, F.; Akbari, S.; Bai, D.; Emadzadeh, D.; Matsuura, T.; Kruczek, B. Improvement of Stability and Performance of Functionalized Halloysite Nano Tubes-Based Thin Film Nanocomposite Membranes. *J. Membr. Sci.* **2018**, *563*, 470−480, DOI: 10.1016/j.memsci.2018.05.070.